Journal of Nuclear Materials 435 (2013) 189–195

Contents lists available at SciVerse ScienceDirect

Journal of Nuclear Materials

journal homepage: www.elsevier.com/locate/jnucmat

Annealing effects on the microstructure and coercive field of two ferritic–martensitic Eurofer steels: A comparative study

V.B. Oliveira [a], M.J.R. Sandim [a], D. Stamopoulos [b], R.A. Renzetti [a], A.D. Santos [c], H.R.Z. Sandim [a,*]

[a] Escola de Engenharia de Lorena, University of Sao Paulo, 12600-970 Lorena-SP, Brazil
[b] Institute of Advanced Materials, Physicochemical Processes, Nanotechnology and Microsystems, NCSR "Demokritos", 153-10 Athens, Greece
[c] Instituto de Física, University of Sao Paulo, 05314-970 São Paulo-SP, Brazil

ARTICLE INFO

Article history:
Received 10 April 2012
Accepted 3 December 2012
Available online 21 December 2012

ABSTRACT

Reduced-activation ferritic–martensitic steels are promising candidates for structural applications in future nuclear fusion power plants. Oxide dispersion strengthened ODS-Eurofer and Eurofer 97 steels were cold rolled to 80% reduction in thickness and annealed in vacuum for 1 h from 200 to 1350 °C to evaluate both their thermal stability and magnetic behavior. The microstructural changes were followed by magnetic measurements, in particular the corresponding variation of the coercive field (H_c), as a function of both annealing and tempering treatments. Results show that Y_2O_3 nanoparticles strongly affect the mechanical properties of ODS-Eurofer steel but leave their magnetic properties fairly unchanged when compared with Eurofer-97 steel.

1. Introduction

The interest on reduced-activation ferritic–martensitic (RAFM) steels has increased substantially in recent years in consequence of their special properties such as high irradiation resistance, high mechanical strength, reasonable ductility and low neutron-induced radioactivity. Due to this unique combination of properties, RAFM steels are potential candidates for high temperature structural applications in future nuclear fusion reactors [1–4]. In special, the possibility of replacing conventional RAFM steels (non-ODS) by oxide dispersion strengthened (ODS) steels may allow the increase the operating temperature from 550 °C up to 650 °C or even higher [2,5].

In an earlier paper, we have investigated the annealing effects on microstructure and coercive field of 9%Cr-ODS-RAFM Eurofer steel developed for the requirements of the European fusion technology program [6]. In this material, hereafter named ODS-Eurofer steel, both nanoscale Y_2O_3 and coarse $M_{23}C_6$ (M = Cr, Fe) particles are found dispersed in the ferritic Fe–Cr matrix [7–9]. The oxide particles have sizes of about 12 nm or even smaller, while the carbide particles have sizes of about 0.2–1 μm [4,10].

Concerning the thermal stability of ODS-Eurofer steel, it was found that the oxide particles play an important role with regard to its annealing behavior. In despite of the presence of coarse carbide particles which stimulated primary recrystallization, the influence of Y_2O_3 is much more pronounced, preventing primary recrystallization [6,7]. The main results on the microstructural changes of ODS-Eurofer steel upon annealing followed by magnetic measurements (coercive field), are reported in Ref. [6].

In general, magnetic properties are very sensitive to detect microstructural changes. Such magnetic measurements have the advantage of being non-destructive in nature and have high sensitivity to detect bulk microstructural changes related to solid-state reactions like recovery and recrystallization and any other phase transformation [11,12]. From the literature it is known that the coercive field H_c reflects the amount and strength of pinning of domain walls [13,14]. The coercive field in a polycrystal is strongly dependent on microstructural parameters such as grain size (d) and dislocation density (ρ) [13,14]. Theoretical considerations demonstrate that $H_c \propto \sqrt{\rho}$, and $H_c \propto 1/d$ [11,12]. Besides free dislocations and grain boundaries, domain walls can be pinned by all different kinds of microstructural defects existing in a crystal such as vacancies, solutes, second-phase particles, twin boundaries and many others under the condition that these defects have appropriate size characteristics to match the ones of domain walls [15].

In the present work we investigate Eurofer-97 steel, a non-ODS RAFM Eurofer steel with similar chemical composition of an ODS RAFM Eurofer one, investigated very recently [6]. The thermal stability of Eurofer-97 steel was evaluated within a wide range of annealing temperatures (200 °C up to 1350 °C) based on Vickers hardness, crystallographic texture, and coercive field measurements. The results were compared with those previously reported for ODS-Eurofer steel [6]. The main differences between these two steels are the presence of a fine dispersion of Y-based particles and distinct amounts of carbon and nitrogen. The present comparative study allows us to have a deeper insight on the role played by both

* Corresponding author. Tel.: +55 12 3159 9916; fax: +55 12 3153 3006.
E-mail addresses: hsandim@demar.eel.usp.br, hsandim@uol.com.br (H.R.Z. Sandim).

0022-3115/$ - see front matter © 2012 Elsevier B.V. All rights reserved.
http://dx.doi.org/10.1016/j.jnucmat.2012.12.017

Y_2O_3 nanoparticles and the coarse $M_{23}C_6$ particles on the microstructure and on magnetic properties of these RAFM Eurofer steels, unveiling that carefully chosen alloying can selectively modulate the former, without affecting the latter. We believe that these results are relevant to understand the mechanical and magnetic properties of RAFM-Eurofer steels, thus making feasible their optimization for future fusion power plant applications.

2. Experimental

The nominal composition of Eurofer-97 steel used in the present investigation was 9Cr–1.1W–0.125Ta–0.25V–0.105C–0.6Mn–0.036N (wt.%). Its chemical composition is similar to ODS-Eurofer steel 9Cr–1W–0.08Ta–0.2V–0.07C–0.4Mn–0.0278N–0.3Y_2O_3 (wt.%) [6]. Both steels were received in the as-tempered condition (about 750 °C for 2 h). The as-tempered Eurofer-97 steel was cold rolled to 80% thickness reduction in multiple passes. Samples were annealed in vacuum from 200 °C up to 1350 °C for 1 h followed by air cooling. Only the specimens annealed in the austenite phase field (850–1350 °C) followed by air cooling were tempered at 550 °C and 750 °C for 2 h in vacuum in sealed glass. Vickers microhardness testing was performed on the longitudinal sections of polished samples using a load of 200 g for 30 s. A LEO 1450-VP scanning electron microscope (SEM) was used to image the microstructure in the backscattered electrons mode operated at 20 kV. The grain size of Eurofer-97 steel after primary and secondary recrystallization was determined using the linear intercept method [16]. About 300 and 250 recrystallized grains were counted, respectively. Macrotexture data at the grain scale were obtained by the X-ray pole figures (1 1 0), (2 0 0), (2 1 1) which were measured from the middle layer in thickness and used to calculate the orientation distribution function (ODF). The pole figures were obtained with a MPD Philips diffractometer using Cu Kα radiation (40 kV, 20 mA). ODFs were calculated for Eurofer-97 steel using the popLA software package. The magnetic measurements were performed at room temperature using a vibrating sample magnetometer (VSM) from EG&G Princeton Applied Research. Two sets of samples were cut into approximate dimensions $5 \times 3 \times 1{,}8\ mm^3$, with the larger dimension taken at two conditions, viz. parallel and perpendicular to the rolling direction (RD). Accordingly, the magnetization curves were obtained with the external field parallel to the larger dimension of the sample (5 mm), in order to obtain the hysteresis loops for two field configurations, i.e. the magnetic field applied either parallel or perpendicular to the RD. The maximum applied field was 16 kOe and the hysteresis loops were carried out using the following sweep rates: 0.4 kOe/min for $|H| < 0.5$ kOe, 1.8 kOe/min for $0.5 < |H| < 5$ kOe and 10 kOe/min for $6 < |H| < 16$ kOe. From the hysteresis loop the coercive field can be determined with an accuracy of ±5 Oe. The experimental procedures described above were performed using the same methodology adopted for ODS-Eurofer steel reported in Ref. [6]. Thus, the comparison of the data obtained in these two specimens is straightforward.

3. Results and discussion

3.1. Microstructure

The softening behavior of Eurofer-97 steel is displayed in Fig. 1. The correspondent data for ODS-Eurofer steel, already reported in Ref. [6], is also displayed to ease comparison. Both materials differ in terms of their annealing behavior. For the same rolling strain, at room temperature, ODS-Eurofer steel is harder than Eurofer-97 due to the more intensive work hardening found in ODS materials

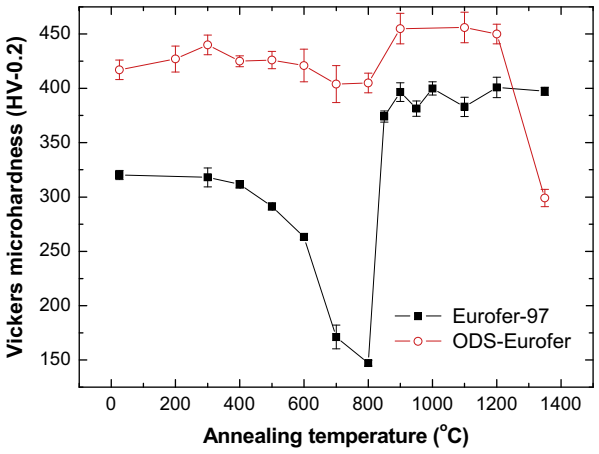

Fig. 1. Softening behavior of 80% cold-rolled Eurofer-97 and ODS-Eurofer steels followed by 1 h annealing at several temperatures up to 1350 °C.

[17]. Concerning the results found in the ferritic-phase field, i.e., for annealing temperatures up to 800 °C, Eurofer-97 steel softens more than ODS-Eurofer steel in the investigated temperature range. Such characteristic can be attributed to the presence of Y-based particles in ODS-Eurofer steel that prevents recrystallization [6,7]. On the other hand, hardness remains nearly unchanged in Eurofer-97 steel until 400 °C and experiences a noticeable softening in the temperature range between 400 and 800 °C. These characteristics enable us to estimate the temperature ranges where static recovery and discontinuous recrystallization are the predominant softening processes in Eurofer-97 steel being, $T < 400$ °C and 400 °C $< T <$ 650 °C, respectively.

A closer inspection at the softening curve of the Eurofer-97 steel displayed in Fig. 1 shows an abrupt drop in hardness between about 650 °C and 800 °C. The reasons for such pronounced softening can be explained after metallographic examination. Fig. 2 shows the microstructures of Eurofer-97 steel annealed for 1 h at three distinct temperatures (650, 700 and 800 °C). The rolling direction (RD) is parallel to the scale bar in all micrographs. From Fig. 2a it is possible to visualize a few recrystallization nuclei in the sample annealed at 650 °C. These elongated grains differ from the fine grains after primary recrystallization in terms of size. Annealing at higher temperatures (700 °C) promotes significant changes in the microstructure due to secondary recrystallization, as shown in Fig. 2b and c.

Understanding the microstructure evolution of Eurofer-97 steel upon annealing depends strongly on knowing its initial metallurgical condition. Regarding size and nature of the particles found in both steels, recent TEM investigations reported in the literature showed that the microstructure of Eurofer-97 steel in the as-received condition (hot rolled and tempered) contains mostly $M_{23}C_6$ at lath boundaries and a few Ta- and V-rich carbides in the interior of the martensite laths [18,19]. Fernández et al. reported other types of Ta- or V-rich precipitates (MX-type) in Eurofer-97 steel, with sizes ranging from 8 to 40 nm, whereas $M_{23}C_6$ precipitates have variable size in the range 25–210 nm [18]. In a recent paper, Klimenkov et al. reported the presence of $M_{23}C_6$, TaC, VN and TiN precipitates by performing intensive TEM investigation in Eurofer-97 steel in the tempered condition [19]. It is worth mentioning that the material investigated by Klimenkov et al. and ours have very similar chemical compositions. $M_{23}C_6$ particles had sizes ranging between 30 and 300 nm with an average size of 120 nm whereas other particles were even smaller. TaC and TiN particles are found dispersed throughout the ferritic matrix whereas VN and $M_{23}C_6$ ones are found at grain and lath boundaries [19]. These

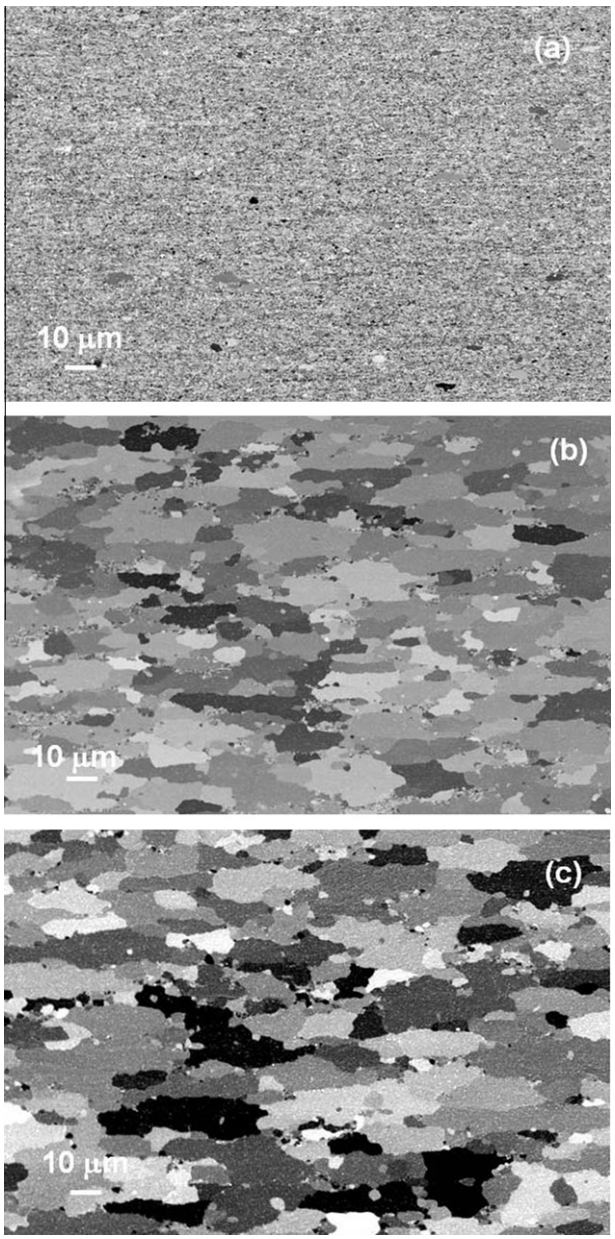

Fig. 2. Microstructure of Eurofer-97 steel annealed for 1 h at three distinct temperatures: (a) 650, (b) 700 and (c) 800 °C (SEM).

compounds (TiN, TaC, VN) have very low enthalpies of formation and remain rather stable after annealing in the range 200–800 °C, i.e. they undergo neither dissolution nor other phase transformation within this temperature range.

According to Lu et al. $M_{23}C_6$ and Y_2O_3 particles are the predominant phases in ODS-Eurofer steel besides the Cr–Fe matrix [20]. Klimiankou et al. reported the results of composition of $M_{23}C_6$ particles in ODS-Eurofer steel as $(Cr_{12}Fe_{10}W)C_6$ in a plate processed in the same batch of ours reported in Ref. [6] indicating that part of chromium is replaced by tungsten atoms in the compound [10]. Regarding nanosized Y_2O_3 particles in ODS materials, literature also reported important results obtained from atom-probe tomography (APT) experiments showing that part of yttrium in the outer shells of former Y_2O_3 particles is replaced by other atoms such as titanium, vanadium, and chromium depending on alloy composition [21]. These results are in agreement with those reported by Klimenkov and co-authors using analytical TEM investigations in nanosized oxide clusters with sizes of about 10 nm [22].

Secondary recrystallization or abnormal grain growth is a solid-state reaction driven by the reduction of the grain boundary surface energy in polycrystals [23]. Strong crystallographic texture, finely dispersed particles, and surface effects caused by the specimen size (thin sheets) favor secondary recrystallization in polycrystals. In the present case, the first two factors are present. Eurofer-97 steel was cold rolled to 80% reduction in thickness corresponding to a strain $\varepsilon = 1.6$. Ferritic steels deformed to large strains develop intense crystallographic texture [24,25]. Following primary recrystallization, the crystallographic texture remains strong in Eurofer-97. Detailed results of X-ray diffraction texture measurements in Eurofer-97 steel will be presented and discussed in Section 3.2.

Fine particles exert important pinning effects on grain boundaries (Zener pinning). Only weakly pinned grain boundaries with high mobility are able to migrate developing a size advantage at the early stages of secondary recrystallization. TaC particles, for instance, are very stable and display low propensity to coarsening when austenitized below 1050 °C [26]. It is worth mentioning that our Eurofer-97 steel samples were normalized at 980 °C for 15 min to avoid intensive austenite grain growth followed by tempering at 760 °C for 90 min [27].

The nucleation of secondary recrystallized grains depends very much on local conditions regarding size, nature and spatial distribution of fine particles. As discussed earlier, fine particles of TaC, TiN, and VN are typically found in Eurofer-97 [18,19] and more recently reported in China low activation martensitic (CLAM) steels [26] in the tempered condition and may act as important pinning obstacles for grain boundary migration. On the other hand, coarse $M_{23}C_6$ carbide particles favor primary recrystallization in cold-rolled Eurofer-97 steel up to 650 °C via particle stimulated nucleation (PSN) mechanism. For a detailed discussion on this mechanism of recrystallization see Ref. [23].

The Eurofer-97 steel used in the present investigation has very similar composition and microstructure in the as-received condition when compared to [19]. Hence it is reasonable to admit that finely dispersed particles and intense deformation texture developed during large straining exist and the necessary conditions for secondary recrystallization are fulfilled. Grain size has significant effects on mechanical, electrical, and magnetic properties of polycrystalline materials. The grain size distributions for Eurofer-97 steel following primary and secondary recrystallization are shown in Fig. 3. Annealing at 800 °C for 5 min causes full primary recrystallization in 80% cold-rolled Eurofer-97 steel yielding an ultra-fine ferrite grain structure with average grain size of about 0.7 μm (Fig. 3a). After secondary recrystallization, the average grain size is 25 μm (Fig. 3b), about one order of magnitude larger than after primary recrystallization. This significant change in grain size is the major cause for the pronounced softening between 650 and 800 °C. Contrastingly, grain growth showed no significant effects in the magnetic properties as will be discussed in Section 3.3.

For annealing temperatures above 800 °C, both steels experience a martensitic transformation upon air cooling. Such transformation is characterized by a substantial increase in dislocation density to compensate crystal lattice distortion, by the appearance of a large number of interfaces and by the dissolution of the $M_{23}C_6$ carbide particles. Due to the martensitic transformation both materials present noticeable hardening, which is more marked in Eurofer-97 steel in terms of percentage increase. Hardness remains almost unchanged when annealing is performed between 900 and 1200 °C in ODS-Eurofer steel followed by a significant drop at 1350 °C. Such drop can be attributed to intensive austenite grain coarsening when the steel is annealed at such elevated temperature [6]. Contrastingly, such sharp drop in hardness is not observed in

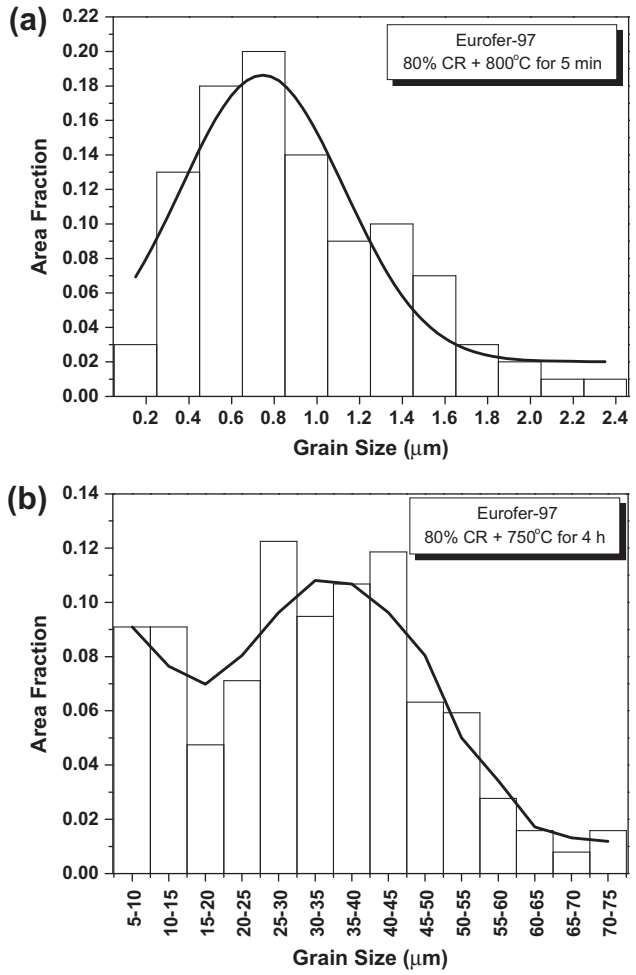

Fig. 3. Grain size distributions of 80% cold-rolled Eurofer-97 steel annealed at: (a) 800 °C for 5 min (primary recrystallization); and (b) 750 °C for 4 h (secondary recrystallization).

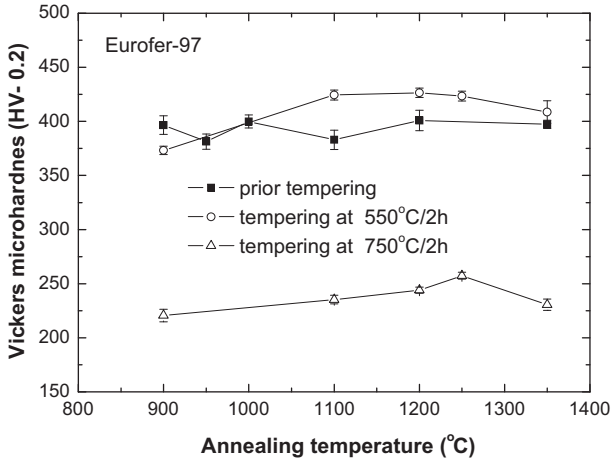

Fig. 4. Vickers hardness values obtained for Eurofer-97 steel annealed in the austenitic field and also tempered at 550 °C and 750 °C for 2 h.

Eurofer-97 steel. For this material, hardness remains nearly unchanged when annealing is performed between 850 and 1350 °C. A possible explanation for such behavior will be provided later on along the presentation of magnetic data.

Fig. 4 shows the effect of tempering on Vickers microhardness of Eurofer-97 steel. Annealing was performed in the range 900–1350 °C whereas tempering was performed for 2 h at 550 °C and 750 °C. In the as-tempered condition, hardness is leveled off at about 380 HV-0.2. Tempering at 750 °C promotes a more substantial softening. However, it must be noticed that samples tempered at 550 °C are slightly harder than the corresponding ones in the as-tempered condition. At light of these results, a possible explanation for the unexpected behavior of hardness of Eurofer-97 steel tempered at 550 °C could be the precipitation of nitrides, in consequence of its higher nitrogen content, when compared with ODS-Eurofer steel. This is consistent with the fact that fine and coherent particles found at the early stages of precipitation are much more effective to strengthen metal alloys than coarser ones found at high tempering temperatures [28]. For comparison, softening was observed in ODS-Eurofer steel in both tempering conditions, being more pronounced at 750 °C [6].

3.2. Crystallographic texture

The crystallographic texture of Eurofer-steel was evaluated in the deformed state and after both primary and secondary recrystallization. Results showing the main texture components and their intensities are shown in Fig. 5. Qualitative and quantitative analyses were carried out using the orientation distribution functions (ODFs) in sections of $\varphi_2 = 0°$ and 45° as they contain the most relevant texture components of Fe–Cr steels [24]. In Fig. 5 a key to the main orientations is also included to ease the identification of the texture components found in section $\varphi_2 = 45°$ (Bunge notation).

Results for the sample in the as-deformed condition (Fig. 5a and b) show texture components belonging to α and γ fibers commonly found in cold-rolled bcc steels. The α-fiber refers to all orientations with a common ⟨1 1 0⟩ axis along the rolling direction RD. The γ fiber refers to all grains with a common ⟨1 1 1⟩ axis parallel to the sheet normal. The α fiber has a maximum close to {1 1 3}⟨1 1 0⟩ whereas the γ fiber is complete with maxima centered between $\{1\,1\,1\}\langle 1\,\bar{2}\,1\rangle$ and {1 1 1}⟨1 1 0⟩. Orientations spreading around the rotated cube component {1 0 0}⟨1 1 0⟩ are also present. Following primary recrystallization (Fig. 5c and d), the {1 0 0}⟨1 1 0⟩ (rotated cube) is still noticeable but weaker and the main texture components of both α and γ fibers are similar to those found in the deformed sample. Not only grain size changes dramatically after secondary recrystallization. Texture also changes as shown in Fig. 5e and f. The rotated-cube component almost vanishes and a sharp $\{1\,1\,1\}\langle 1\,\bar{2}\,1\rangle$ texture develops in Eurofer-97 steel sheets.

3.3. Magnetic properties

Concerning the magnetic properties, Fig. 6 depicts the coercive field (H_c) as a function of the annealing temperature for Eurofer-97 steel together with the correspondent data for ODS-Eurofer steel [6]. Because of the many possibilities of how domain walls can interact with pinning obstacles in both steels, the correlation between microstructural evolution and magnetic properties is not straightforward. A deeper analysis could also take into account how particles are distributed, i.e. forming clusters, precipitated at interfaces (lath and grain boundaries) or uniformly dispersed. For sake of simplicity, we divide our analysis in two regions where isothermal annealing is performed, i.e. the ferritic and the austenitic phase fields.

In the ferritic phase there is a noticeable difference regarding hardness levels of both steels and their corresponding annealing behavior (see Fig. 1). In contrast, comparing Figs. 1 and 6, there is no significant difference concerning their coercive field values, H_c below 800 °C. This means that (i) the presence of Y_2O_3

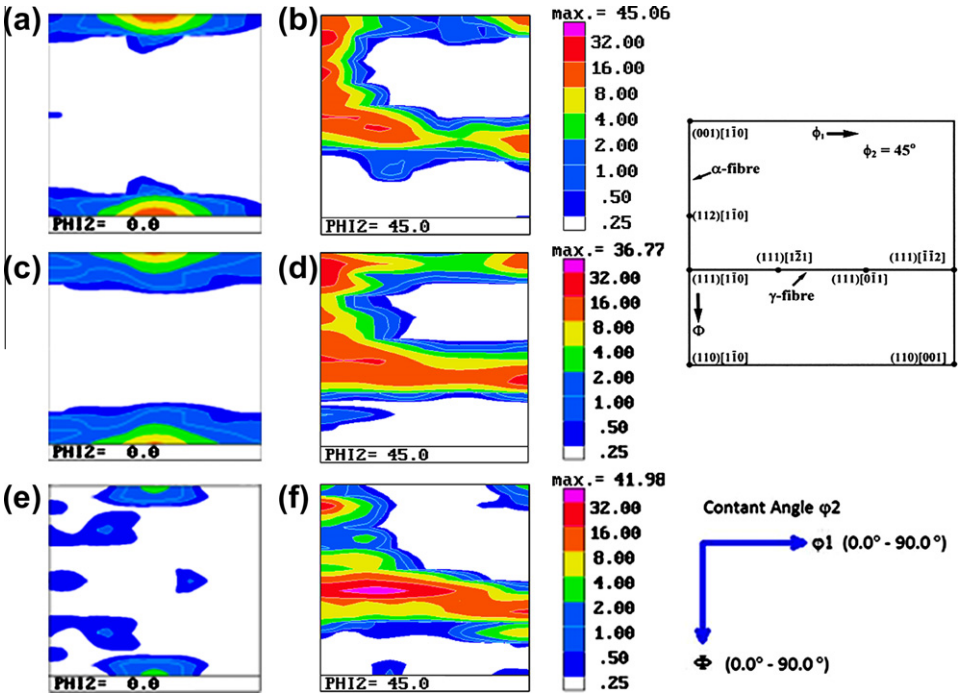

Fig. 5. Microtexture of Eurofer-97 steel in several metallurgical conditions: (a and b) 80% cold-rolled; (c and d) annealed at 750 °C for 5 min (full primary recrystallization); (e and f) annealed at 750 °C for 4 h (full secondary recrystallization).

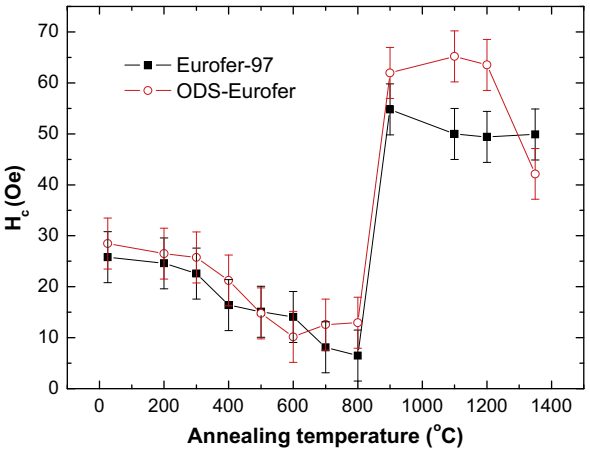

Fig. 6. H_c values obtained for Eurofer-97 and ODS-Eurofer steels for as-rolled and annealed conditions (field configuration parallel to the rolling direction).

nanoparticles that exist only in the ODS-Eurofer steel and (ii) the significantly different mechanical properties and underlying microstructures are not the main influence on the coercive field for these steels. These results strongly suggest that, for such annealing temperature range, the presence of $M_{23}C_6$ carbide and other minor phases with sizes in the range and slightly below 1 μm is the most important parameter that influences the coercive field in both steels. Obviously, the Y_2O_3 nanoparticles cannot be direct pinning centers for magnetic domain walls. From our point of view these results are quite interesting because they unveil means to *selectively* tailor either the mechanical or magnetic properties in an independent way, thus making feasible the optimization of the respective technical parameters that are important for utilization of these steels in practical applications. For instance, as shown in this comparative study, Y_2O_3 nanoparticles strongly affect the mechanical properties, while the magnetic properties remain almost unchanged.

Above 850 °C, where the martensitic transformation takes place upon subsequent cooling, a significant increase in H_c can be noticed for both steels (Fig. 6). Such increase is similar in magnitude but, in spite of this, in the temperature range between 900 and 1200 °C, H_c values for the investigated steels are clearly different, with the Eurofer-97 steel exhibiting a more 'magnetically soft' character. For annealing at 1350 °C a noticeable difference concerning H_c behavior for the investigated steels is observed, in nice agreement with what is already observed for hardness. $M_{23}C_6$ particles are dissolved during annealing of both steels in the austenitic phase field. Therefore, when annealing is performed in the austenitic field, in consequence of the martensitic transformation, other microstructural parameters such as free dislocations and interfaces (lath boundaries) have more influence on the coercive field, as this is evidenced by the almost scaling of the Vickers microhardness with the coercive field. The values of the dislocation density have been recently evaluated in samples of ODS-Eurofer steel deformed by cold rolling to 80% reduction in thickness followed by annealing at 1100 °C and 1350 °C for 1 h with subsequent air cooling being, respectively, 7.0×10^{15} and 5.0×10^{15} m^{-2} [29]. For purpose of comparison, the dislocation density for the same steel annealed at 800 °C for 1 h was 5.0×10^{15} m^{-2} [29]. Interestingly, in ODS-Eurofer steel, the variation observed in dislocation density [29] is directly reflected in the respective modulation of the coercive field, H_c.

In line with the discussion made above, one issue that has to be resolved is how to tune independently the mechanical and magnetic properties. Up to now the effect of the nanodispersion of Y_2O_3 particles in the coercive field was unclear. From Fig. 6 it is observed a noticeable drop in H_c for ODS-Eurofer steel at 1350 °C, while H_c remained constant for Eurofer-97 steel. In a previous study concerning ODS-Eurofer steel, the sharp drop of both hardness and H_c at 1350 °C has been attributed to intensive austenite grain coarsening [6]. It was also argued that when annealing is performed at such high temperature, the fine dispersion of Y_2O_3 particles cannot prevent grain boundary migration allowing subsequent grain growth [6]. At light

of new experimental evidences displayed in Figs. 1 and 6, a new question emerges concerning the likely annealing effects on Y_2O_3 particles. Such question concerns with possible coarsening of the originally nanoscaled Y_2O_3 particles at 1350 °C. It has been reported that no significant changes in size of Y-based particles were observed for short annealing times at 800 °C [7]. To the best of our knowledge, literature does not report the annealing effects on Y-based particles at either higher temperatures or extended annealing times.

Further investigations of these materials with experimental techniques that can provide information on the size of magnetic domains and domain walls are of paramount importance since, based on size-matching arguments, we will be able to figure out which one of the various imperfections (interfaces, nanosized Y_2O_3, other microsized particles etc.) of crystal structure can act as efficient pinning centers of the coexisting magnetic structure. This comparison will ultimately reveal the connection between crystal/mechanical and magnetic properties. Neutron scattering that probes the bulk magnetic properties and magnetic force microscopy that only probes the surface magnetic domain configuration could be the techniques of choice for these future investigations.

Other interesting differences between the two investigated steels emerge when we compare their hardness and magnetic behavior after tempering. In the tempered state, the microstructure of ODS-Eurofer steel consists of a ferritic matrix, nanosized Y_2O_3 particles, a minor fraction of TaC and VN and coarse $M_{23}C_6$ carbides [6]. Such microstructure, except for the presence of Y-based particles, is similar to Eurofer-97 steel following tempering.

Regarding the tempering effects on magnetic properties, Fig. 7 shows the results of H_c in Eurofer-97 steel annealed in the austenitic range followed by tempering at 550 and 750 °C. The corresponding results prior tempering are included for reference. From Fig. 7 it was observed that H_c decreases after tempering and such decrease is more pronounced for the samples tempered at higher temperature (750 °C). From a comparison of Figs. 4 and 7, a striking result is that, for Eurofer-97 steel tempered at 550 °C, coercive field and hardness have opposite trends. For tempered samples at 550 °C, in spite of increasing hardness, the coercive field presents a noticeable decrease. On the other hand, for tempered samples at 750 °C, both H_c and hardness decrease, although the coercive field percentage decrease is more pronounced. For example, for the sample annealed at 900 °C, the percentage decreases found for H_c and Vickers microhardness, are about 80% and 40%, respectively, after tempering at 750 °C. The results of Fig. 4 suggests that, for Eurofer-97 steel, besides intensive dislocation annihilation and precipitation of $M_{23}C_6$ carbides, tempering also leads to precipitation of nitrides. The effect of such second phase particles (both carbides and nitrides) on pinning of magnetic domain walls and, consequently, on coercive field, depends on the relative magnitude of their sizes (radius R) in comparison with the domain wall thickness (δ) [15]. According to Arzt [15], if $R \ll \delta$, $H_c \propto R$ while in the case of $R \gg \delta$, $H_c \propto 1/R$. The maximum value of H_c is expected when $R \approx \delta$ [15]. On the other hand, the thermally-activated dislocation annihilation under tempering contributes to a decrease in H_c following the relationship $H_c \propto \sqrt{\rho}$ [11,12]. The competition or coupling of the different contributions for pinning of domain walls discussed above determine the overall magnitude of H_c, the coercive field. For tempering at higher temperatures it is expected that the size of second phase particles becomes larger [28]. Whatever is the ratio between their sizes and δ, from Fig. 7 we see that the coupling of the different contributions for pinning of domain walls leads to a noticeable decrease of H_c for isothermal tempering at both 550 and 750 °C. Concerning the coercive field, a similar behavior was verified for the ODS-Eurofer steel samples annealed in the austenitic field, followed by isothermal tempering at same temperatures [6]. However, the coercive field decrease ratio is more pronounced in Eurofer-97 steel.

Regarding Eurofer-97 steel, going back to the comparison between Figs. 4 and 7, the results suggest that for tempering at 550 °C the small size of the precipitates contribute for hardening of the material whereas at same time the material becomes 'magnetically softer'. Therefore, for tempering at 750 °C, the higher decrease of H_c in comparison to hardness certainly can be also related to size effects. It must be noticed that we have observed a decrease in both hardness and coercive field for the two chosen tempering conditions (550 and 750 °C) in ODS-Eurofer samples [6]. Also in this case, the coercive field decrease ratio promoted by isothermal tempering was higher in comparison with the observed in terms of hardness.

The possible existence of anisotropy in the coercive field properties was also investigated. Fig. 8 shows the values of coercive field obtained for a magnetic field applied both parallel and perpendicular to the rolling direction (RD). From this figure it is seen that no significant differences were found for both field configurations in spite of the strong texture developed during processing of Eurofer-97 steel, as previously observed for ODS-Eurofer steel [6]. Though there is no actual difference we note that in Figs. 6 and 7 the coercive field was obtained for applied field parallel to the RD.

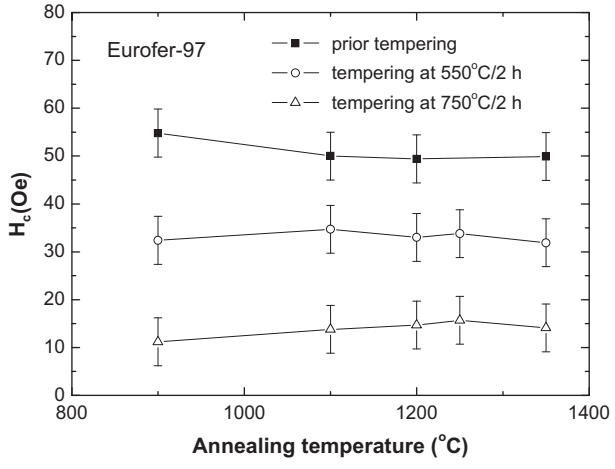

Fig. 7. H_c values obtained for Eurofer-97 steel annealed at austenitic field and also tempered at 550 °C and 750 °C for 2 h (field configuration parallel to the rolling direction).

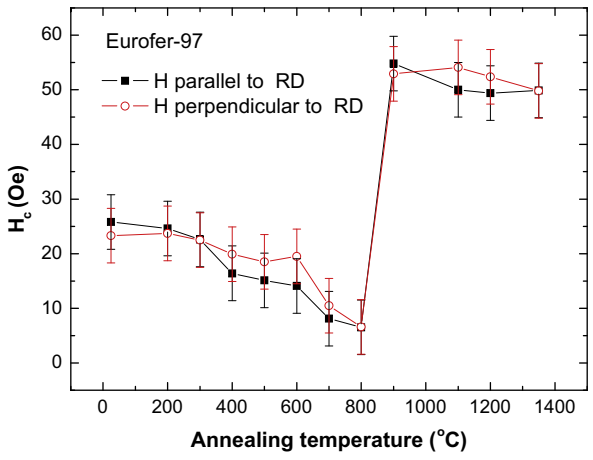

Fig. 8. H_c values for Eurofer-97 steel for both field configurations: applied parallel and perpendicular to the rolling direction.

4. Summary and conclusions

The microstructure evolution of two RAFM steels during isothermal annealing from 200 °C up to 1350 °C was compared. Based on both Vickers microhardness and coercive field measurements, in addition to metallographic inspection, the following conclusions can be drawn:

(1) The two steels display rather distinct annealing behaviors in the ferritic phase field. Softening is much less pronounced in ODS-Eurofer steel due to the presence of a fine and stable dispersion of Y_2O_3 that allows only partial recrystallization. Contrastingly, Eurofer-97 readily undergoes discontinuous recrystallization starting at about 500 °C. Secondary recrystallization becomes pronounced above 650 °C for the latter steel.
(2) The final grain size after secondary recrystallization is about one order of magnitude larger than after primary recrystallization. This significant change in grain size explains the pronounced softening experienced by Eurofer-97 after secondary recrystallization in the range of 650–800 °C. On the other hand, magnetic properties in Eurfer-97 steels remained nearly unchanged following secondary recrystallization.
(3) The crystallographic texture of Eurofer-97 steel in the as-deformed and fully-recrystallized conditions are quite similar showing texture components commonly found in ferritic Fe–Cr steels. The α fiber has a maximum close to $\{1\,1\,3\}\langle 1\,1\,0\rangle$ whereas the γ fiber is complete with maxima centered between $\{1\,1\,1\}\langle 1\,\bar{2}\,1\rangle$ and $\{1\,1\,1\}\langle 1\,1\,0\rangle$. After secondary recrystallization annealing at 750 °C for 4 h, textures changes significantly with strengthening of the $\{1\,1\,1\}\langle 1\,\bar{2}\,1\rangle$ component and corresponding weakening of the rotated-cube component.
(4) Despite the noticeable differences concerning their softening behavior below 800 °C, the corresponding magnetic behavior of ODS-Eurofer and Eurofer-97 steels regarding their coercive fields is quite similar. The results suggest that, for such temperature range, the coercive field is dominated by the $M_{23}C_6$ carbides and other minor phase particles with sizes below 1 μm.
(5) In the austenitic field the main difference between the two investigated steels is concerning the annealing at 1350 °C. For the Eurofer-97 steel, both hardness and H_c remains almost constant for annealed samples in the temperature range 850–1350 °C. In contrast, for the ODS-Eurofer there is a drastic drop of these properties after annealing at 1350 °C. Such behavior can be attributed either to intensive austenite grain growth or due to coarsening of the Y_2O_3 particles (Ostwald ripening).
(6) In the austenitic field there is a good qualitative agreement between Vickers microhardness and magnetic coercive field values for both investigated steels. Such feature is also valid for tempered samples of ODS-Eurofer steel. However, for the Eurofer-97 steel, depending on the tempering temperature, microhardness and coercive field have opposite trends, possibly due to different size effects caused by precipitation of fine vanadium nitride particles.
(7) As a general concluding comment, Y_2O_3 nanoparticles strongly affect the mechanical properties of ODS-Eurofer steel but leave their magnetic properties fairly unchanged. This could provide us new means to tailor either the mechanical or magnetic properties in an independent way, thus enhancing the compatibility of these steels with the different needs of a wider spectrum of practical applications.

Acknowledgments

This work was partially supported by the Brazilian Financial Agency FAPESP (Grant Number 10/51.759-9). The authors also thank to CAPES and CNPq (Brazil) for partial financial support and to Dr. A. Möslang and to Dipl.-Ing. R. Lindau (KIT, Karlsruhe, Germany) for supplying the steels for this investigation. Authors are also grateful to Prof. R.E. Bolmaro (IFIR, Rosário, Argentina) for his kind assistance in performing the X-ray texture measurements.

References

[1] K. Ehrlich, Fusion Eng. Des. 56–57 (2001) 71–82.
[2] R. Lindau, A. Möslang, M. Rieth, M. Klimenkou, E. Materna-Morris, A. Alamo, A.-A.F. Tavassoli, C. Caryon, A.-M. Lancha, P. Fernandez, N. Baluc, R. Schäublin, E. Diegele, G. Filacchioni, J.W. Resman, Eng. Des. 75–79 (2005) 989–996.
[3] A. Möslang, E. Diegele, M. Klimenkou, R. Lässer, R. Lindau, E. Lucon, E. Materna-Morris, C. Petersen, R. Pippan, J.W. Renaman, M. Rieth, Nucl. Fusion 45 (2005) 649–655.
[4] C.A. Williams, E.A. Marquis, A. Cerezo, G.D.W. Smith, J. Nucl. Mater. 400 (2010) 37–45.
[5] A. Möslang, Ch. Adelhelm, R. Heidinger, Int. J. Mater. Res. 99 (2008) 1045–1054.
[6] R.A. Renzetti, H.R.Z. Sandim, M.J.R. Sandim, A.D. Santos, A. Möslang, D. Raabe, Mater. Sci. Eng. A 528 (2011) 1442–1447.
[7] H.R.Z. Sandim, R.A. Renzetti, A.F. Padilha, D. Raabe, M. Klimenkov, R. Lindau, A. Möslang, Mater. Sci. Eng. A 527 (2010) 3602–3608.
[8] R. Schaeublin, T. Leguey, P. Spätig, N. Baluc, M. Victoria, J. Nucl. Mater. 307–311 (2002) 778–782.
[9] M. Klimiankou, R. Lindau, A. Möslang, J. Nucl. Mater. 329–333 (2004) 347–351.
[10] M. Klimiankou, R. Lindau, A. Möslang, J. Nucl. Mater. 367–370 (2007) 173–178.
[11] A. Martínez-de Guerenu, F. Arizti, M. Dias-Fuentes, I. Gutiérrez, Acta Mater. 52 (2004) 3657–3664.
[12] M. Oyarzábal, K. Gurruchaga, A. Martínez-de-Guerenu, I. Gutiérrez, ISIJ Int. 47 (2007) 1458–1464.
[13] B.D. Cullity, Introduction to Magnetic Materials, Addison-Wesley, Boston, 1972.
[14] M.J. Sablik, J. Appl. Phys. 89 (2001) 7254–7256.
[15] E. Arzt, Acta Mater. 46 (1998) 5611–5626.
[16] ASTM E 112, Test Method for Determining Average Grain Size. Annual Book of ASTM Standards, ASTM International, 2005.
[17] D. Häussler, B. Reppich, M. Bartsch, U. Messerschmidt, Mater. Sci. Eng. A309–310 (2001) 500–504.
[18] P. Fernández, A.M. Lancha, J. Lapeña, M. Serrano, M. Hernández-Mayoral, J. Nucl. Mater. 307 (2002) 495–499.
[19] M. Klimenkov, R. Lindau, E. Materna-Morris, A. Möslang, Prog. Nucl. Energy 57 (2012) 8–13.
[20] Z. Lu, R.G. Faulkner, N. Riddle, F.D. Martino, K. Yang, J. Nucl. Mater. 386–388 (2009) 445–448.
[21] E.A. Marquis, Appl. Phys. Lett. 93 (2008). 181904–181904-3.
[22] M. Klimenkov, R. Lindau, A. Möslang, J. Nucl. Mater. 386–388 (2009) 553–556.
[23] F.J. Humphreys, M. Hatherly, Recrystallization and Related Annealing Phenomena, Pergamon, 1996.
[24] D. Raabe, K. Lücke, Mater. Sci. Technol. 9 (1993) 302–312.
[25] B. Hutchinson, Philos. Trans. R. Soc. London A 357 (1999) 1471–1485.
[26] X. Zhi-xin, Z. Chi, H. Qun-ying, L. Shao-jun, L. Zhao-dong, Y. Zhi-gang, J. Iron Steel Res. Int. 18 (2011) 47–52.
[27] E. Materna-Morris et al., Final report on the EFDA task TW4-TTMS-005 D2, structural material Eurofer97-2, characterization of rod and plate material: structural, tensile, charpy, and creep properties, FZK Interner, Bericht 31.40.04, November 2007.
[28] G. Gottstein, Physical Foundations of Materials Science, Springer, Berlin, 2004.
[29] R.A. Renzetti, H.R.Z. Sandim, R.E. Bolmaro, P.A. Suzuki, Mater. Sci. Eng. A 534 (2012) 142–146.